

**Fermi National Accelerator Laboratory**

**FERMILAB-TM-2096**

**Electro-Optic Measurement of the Wake Fields of 16 MeV Electron  
Bunches**

M.J. Fitch et al.

*Fermi National Accelerator Laboratory  
P.O. Box 500, Batavia, Illinois 60510*

November 1999

## **Disclaimer**

*This report was prepared as an account of work sponsored by an agency of the United States Government. Neither the United States Government nor any agency thereof, nor any of their employees, makes any warranty, expressed or implied, or assumes any legal liability or responsibility for the accuracy, completeness, or usefulness of any information, apparatus, product, or process disclosed, or represents that its use would not infringe privately owned rights. Reference herein to any specific commercial product, process, or service by trade name, trademark, manufacturer, or otherwise, does not necessarily constitute or imply its endorsement, recommendation, or favoring by the United States Government or any agency thereof. The views and opinions of authors expressed herein do not necessarily state or reflect those of the United States Government or any agency thereof.*

## **Distribution**

*Approved for public release; further dissemination unlimited.*

## **Copyright Notification**

*This manuscript has been authored by Universities Research Association, Inc. under contract No. DE-AC02-76CH03000 with the U.S. Department of Energy. The United States Government and the publisher, by accepting the article for publication, acknowledges that the United States Government retains a nonexclusive, paid-up, irrevocable, worldwide license to publish or reproduce the published form of this manuscript, or allow others to do so, for United States Government Purposes.*

# Electro-optic Measurement of the Wake Fields of 16 MeV Electron Bunches

M.J. Fitch<sup>(1,a)</sup>, N. Barov<sup>(2,b)</sup>, J.P. Carneiro<sup>(2,a,c)</sup>, P.L. Colestock<sup>(2,d)</sup>, H.T. Edwards<sup>(2)</sup>,  
K.P. Koepke<sup>(2)</sup>, A.C. Melissinos<sup>(1)</sup> and W.H. Hartung<sup>(2)</sup>

<sup>(1)</sup> *Department of Physics and Astronomy, University of Rochester, Rochester, NY 14627*

<sup>(2)</sup> *Fermi National Accelerator Laboratory, Batavia, IL 60510*

## Abstract

We demonstrate the measurement in the time domain and with picosecond resolution of the high frequency electromagnetic fields generated by a bunched beam of 16 MeV electrons. A birefringent crystal placed 2 cm from the beam is sampled in time by a pulsed laser synchronized with the electron bunch. The electric field waveform has been recorded with substantial structure as late as 2.5 ns after the passage of the bunch.

10/11/99

The development of electron accelerators with ever higher particle density is essential for applications to high energy physics, photon and x-ray sources and free electron lasers. The electrons are produced in short pulses with low emittance that must be preserved during acceleration. Because of unavoidable discontinuities in the beam pipe and accelerating structure, the electrons radiate, exciting wake-fields in the structure. The calculation and measurement of these fields is important because they can lead to energy spread and emittance growth of the beam. Also field measurements can be used to infer the bunch length and particle density of the beam.

Electro-optic (eo) sampling of the wake-fields is quite attractive because it is a non-invasive technique and offers picosecond, or even femtosecond time resolution as long as the probe beam remains synchronized with the electron bunches. In principle it is possible to identify the separate components of the field and to make absolute measurements of the field strength. Applications of eo sampling to high energy particle beams are discussed in refs. [1-4].

Electro-optic sampling is based on the Pockels effect and was introduced by Auston [5] in the 1970's. When an electric field is applied to a certain class of crystals the refractive index ellipsoid is modified, and as a result a retardation (phase shift) is introduced between two orthogonally polarized components of a pulse of light traversing the crystal. This retardation can be detected by observing the change in the polarization of the transmitted light. By using short laser pulses and varying the delay between the "probe" pulse and the pulse that produced the electron bunch, the "pump" pulse, one can sample the time dependence of the electric field.

The Fermilab high-brightness photoinjector [6] consists of a normal conducting r-f gun followed by a 9-cell Nb superconducting cavity, delivering electrons of final energy of 16-18 MeV. The r-f frequency is 1.3 GHz. A high quantum efficiency ( $\eta \sim 1 - 2\%$ ) Cs<sub>2</sub>Te photo-cathode is installed in the r-f gun. The photocathode is driven by UV laser pulses that can be shaped both in space and time. Pulse trains of 1 to 200 bunches (8 nC charge) spaced 1  $\mu$ s apart can be accelerated at a repetition rate of 1 Hz. Details of the gun and beamline design can be found in [6]. The design of the pulse train Nd:glass laser is described in [7]. Focussing and steering elements as well as emittance and energy diagnostics are provided in the beam line. The bunch length was measured to be 17 ps FWHM with a Hamamatsu C5680-21S streak camera looking at optical transition radiation. In the future a magnetic compressor (a chicane of 4 dipoles) will be used to further reduce the bunch length to 3.5 ps. Using a slit mask, the measured (invariant) emittance is estimated to be  $\epsilon \simeq 5\pi$  mm-mr. A schematic of the photoinjector is shown in Fig. 1.

The arrangement used in our experiment is shown schematically in Fig. 2. The laser produces a 1 MHz train of up to 800 pulses in the IR ( $\lambda = 1054$  nm). These pulses of energy  $\sim 100$   $\mu$ J are compressed in a set of gratings to a width of 2-3 ps and then quadrupled to the UV. A streak camera measurement of the UV pulse length gives  $\sigma_t = 1.8$  ps. The UV pulse is now lengthened in a pulse stacker [8] to a flat-top of 10 ps FWHM and sent to the cathode. Part of the unconverted IR is used as the "probe" pulse and is routed to the electro-optic crystal via a variable optical delay stage. The stage can be moved with

sub-picosecond resolution, and with a hollow corner cube retroreflector, maintains pointing stability over its entire range of 3 ns.

The eo crystal is placed in the vacuum in a diagnostic cross in the electron beam pipe; the laser probe pulse propagates normally to the electron beam direction passing through entrance and exit windows. The coordinate convention used is indicated in Fig. 2. The beam propagates along z, y is the upgoing vertical and x-y-z form a right-handed system.

The crystal is a 1.5 mm thick piece of LiTaO<sub>3</sub> of area 7 × 8 mm<sup>2</sup>. It is placed at a distance of 2 cm from the center of the beam pipe with its extraordinary axis (3-axis) in the y-z plane, and rotated 45° relative to the horizontal. The thin dimension of the crystal, its 2-axis, coincides with the x-axis (horizontal); the probe beam *k*-vector is along the x-axis and the polarization vector along the y-axis. The two polarizations of the transmitted beam are analyzed by a cube beam splitter and recorded by two separate fast diodes. A λ/4 plate allows us to balance the two diodes in the absence of a field. This is especially important since in our configuration the crystal exhibits a very large natural birefringence. For more details on eo sampling see ref. [9].

In this configuration we are mainly sensitive to the azimuthal and longitudinal components of the electric field, (*E<sub>y</sub>* and *E<sub>z</sub>*, which are tangential to the crystal surface) and much less to the radial component (*E<sub>x</sub>*, normal to the crystal surface). The phase-shifts induced by the three field components are

$$\begin{aligned} \text{for } E \text{ along } y & \quad \Gamma = 2\pi(l/\lambda)\frac{1}{2}(n_e^3r_{33} - n_o^3r_{31})(E_y/\sqrt{2}) \\ \text{for } E \text{ along } z & \quad \Gamma = 2\pi(l/\lambda)\frac{1}{2}(n_e^3r_{33} - n_o^3r_{31})(E_z/\sqrt{2}) \\ \text{for } E \text{ along } x & \quad \Gamma = 2\pi(l/\lambda)\frac{1}{2}n_o^3r_{22}E_x \end{aligned}$$

Here *l* is the length of the crystal, λ the wavelength and the eo coefficients are given by

$$\frac{1}{2}(n_e^3r_{33} - n_o^3r_{31}) = 115 \times 10^{-12} \text{m/V}$$

$$\frac{1}{2}n_o^3r_{22} = 4 \times 10^{-12} \text{m/V}$$

It is the smallness of *r<sub>22</sub>* as compared to *r<sub>33</sub>* that decreases the sensitivity to the transverse field. Note also that in the absence of an electric field the crystal exhibits natural static birefringence of many waves.

$$\Gamma_s = 2\pi\frac{l}{\lambda}(n_e - n_o) \simeq 7.5(2\pi)$$

Since *n<sub>o</sub>* and *n<sub>e</sub>* are temperature dependent, small changes in temperature introduce significant noise in the measurement of the Pockel's effect. This noise source is absent in geometries with no static birefringence.

We denote by *I<sub>a</sub>*, *I<sub>b</sub>* the intensities transmitted through the two sides of the polarizing beamsplitter. We then adjust the static retardation in the absence of an electric field using

the  $\lambda/4$  plate so that  $I_a = I_b$ , so that in the presence of the field

$$I_{a,b} = \frac{I_0}{2}(1 \pm \sin \Gamma)$$

where  $I_0$  is the incident intensity and  $\Gamma$  the field induced retardation. Thus

$$\sin \Gamma = \frac{I_a - I_b}{I_a + I_b} \equiv R$$

To first order the ratio  $R$  is independent of fluctuations in the laser intensity but it can be affected by pointing errors and changes in the natural birefringence.

The intensities  $I_a, I_b$  were measured with two photodiodes, and since the pulsed signals were broadened by a long cable run, data were taken by recording the integral (area) of the  $I_a$  and  $I_b$  pulses on a Tektronix TDS-640 scope. A LabVIEW program running on a Macintosh handles the data acquisition, recording measurements from the scope and moving the delay stage, at a 1 Hz rate. To provide some signal averaging,  $N$  pairs of  $I_a, I_b$  measurements are taken at each delay step. Offline,  $R$  is computed for these  $N$  values, and then averaged. We found  $N = 4$  to be a good compromise between noise suppression and impractically long scans (stability, drifts). The results for  $R = \sin \Gamma \simeq \Gamma$  are shown in Fig. 3 as a function of the delay between the arrival of the probe pulse and of the electron bunch at the crystal. The origin of the delay is arbitrarily chosen and was placed at the best estimation of the electron bunch arrival time from the measured travel distances. The signal is observed to begin at a delay of  $\sim 100$  ps; increasing (positive) delay implies that the probe arrives after the electron bunch. Four laser pulses were averaged at a given delay and then the delay was incremented by 1 ps. The inset in Fig. 3 shows the first 300 ps on an expanded scale and with 10 laser pulses averaged.

The data show clearly the presence of oscillating electric fields following (in the wake of) the electron bunch. This is to be expected since the beam pipe has several discontinuities. Fig. 4 is the Fourier spectrum of the data record of Fig. 3. We recognize the strongest components at

$$\nu = 12.6 \pm 0.5 \text{ GHz}$$

and

$$\nu = 2.7 \pm 0.2 \text{ GHz}$$

It should be possible to identify these frequencies with resonant modes of the beam pipe structure.

MAFIA calculations [10] for the resonant frequencies in the arms of a diagnostic cross, such as the one in which the crystal was located, predict a frequency

$$\nu = 3.06 \text{ GHz}$$

for an inner diameter  $d = 47.5$  mm. This value is reasonably close to the lower of the observed frequencies,  $\nu = 2.7 \pm 0.2$  GHz. The calculation is carried out under the assumption of

proper electric or magnetic boundaries whereas in reality the arms of the cross ended in glass windows.

The predicted field amplitude for this mode can be estimated from the calculated loss factor

$$k_{||} = \frac{2}{q} \int_{-\infty}^{\infty} dz E_{||}(x, y, z; t)|_{t=s+z} = 0.92 \text{ V/pC}$$

Here we assume that electric and magnetic contributions to the loss factor are equal, and  $q$  is the bunch charge. For a bunch length of 20 ps (6 mm) FWHM and  $q = 8 \text{ nC}$  we find

$$E_{||} \sim 6 \times 10^5 \text{ V/m}$$

Not all of the external field penetrates into the crystal which has a large dielectric constant. From the Fresnel formula at normal incidence the transmitted field is

$$E_t = E_o \frac{2n}{n + n_c}$$

and using  $n_c = \sqrt{\epsilon} \sim 7$ ,  $E_t/E_o = 0.25$ . Thus the tangential field inside the crystal is of order  $E = 1.5 \times 10^5 \text{ V/m}$  giving rise to a retardation  $\sin \Gamma = R = 0.15$ . This value is of the same order as observed and, perhaps accidentally, in close agreement with the measured values.

We are less certain about the origin of the higher frequency components. It is quite possible that they correspond to waveguide modes propagating in the beam pipe. Because the azimuthal symmetry is broken by the four ports in the transverse plane of the diagnostic crosses, we expect that the modes will have  $n = 2(\cos 2\phi)n$  dependence. For the beam diameter  $d = 47.5 \text{ mm}$  the corresponding frequencies for the three lowest  $\text{TE}_{2m}$  modes are

$$\begin{aligned} \text{TE}_{2,1} & \quad \nu = 6.1 \text{ GHz} \\ \text{TE}_{2,2} & \quad \nu = 13.4 \text{ GHz} \\ \text{TE}_{2,3} & \quad \nu = 20.0 \text{ GHz} \end{aligned}$$

These values are in the range of the observed frequencies but further computational and experimental work is needed before a unique identification can be made.

The observed signals scale according to the charge of the bunches and for shorter bunches the ratio of high frequency to low frequency components increases drastically. The quality of the signal was strongly dependent on beam focusing but almost insensitive to steering of the beam, towards or away from the eo crystal. Furthermore, as can be seen from Fig. 3 the Q-factor of these excited modes is low.

These investigations are continuing and an effort will be made to measure the transverse component of the field by using a KD\*P crystal. This could provide a direct measurement in the time domain of the bunch length. We note that in principle it is possible to sample the entire pulse train thus increasing significantly the signal to noise ratio. The technique is applicable to any accelerator as long as the probe pulses are synchronized with the beam bunches.

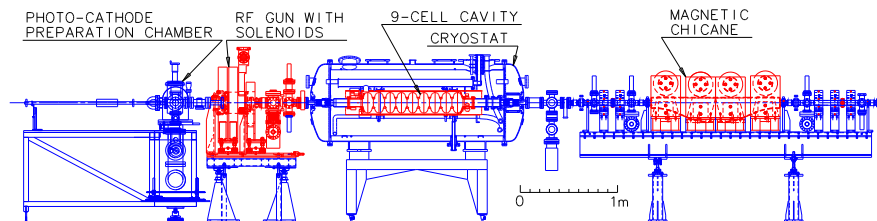
## Acknowledgements

We thank our colleagues on the AØproject for their interest in this project and for their contributions to the effective operation of the photoinjector. We thank the Fermilab Beams Division for continued support. Fermilab is operated by the Universities Research Association under contract with the U.S. Department of Energy. This work was carried out in part under DOE grant DE-FG02-91ER40686.

## References and Notes

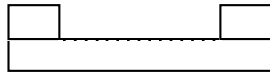
- (*a*) Fermilab Beams Division Graduate Fellow.
- (*b*) University of California at Los Angeles, Los Angeles, CA 90095.
- (*c*) Université d'Orsay, France.
- (*d*) Present address: Los Alamos National Laboratory, Los Alamos, NM 87545.
1. P.J.Channell, "Use of Kerr Cells to Measure RF Fields", Accelerator Theory Note AT-6:ATN-82-1, Los Alamos National Laboratory (1982); Yu. S. Pavlov and N.G. Soloviev, "Formation and measurement of picosecond beams of charged particles", Proc. VIII Particle Accel. Conf. (1982, Protvino, USSR) V2, p. 63-67; M. Geitz, K. Hanke and A.C. Melissinos, "Bunch Length Measurements at TTF1 using Optical Techniques". Internal report TESLA collaboration, DESY (1997).
  2. Y.K. Semertzidis et al. "Electro-optical Detection of Charged Particle Beams". Proceedings of the 1999 Particle Accelerator Conference, New York, NY (1999) p. 490-491. M.J. Fitch et al. "Picosecond Electron Bunch Length Measurement by Electro-Optic Detection of the Wakefield". Ibid. p 2181-2183.
  3. G.M.H. Knippels, X. Yan, A.M. MacLeod, W.A. Gillespie, M. Yasumoto, D. Oepts, and A.F.G. van der Meer, "Generation and Complete Electric-Field Characterization of Intense Ultrashort Tunable Far-Infrared Laser Pulses". Phys. Rev. Lett. 83, 1578 (1999).
  4. D. Oepts, G.M.H. Knippels, X. Yan, A.M. MacLeod, W.A. Gillespie, A.F.G. van der Meer, "Picosecond electron-bunch length measurement using an electro-optic sensor". To appear in proceedings of FEL '99 Conference held at DESY.
  5. D.H. Auston. Appl. Phys. Lett. 26, 101 (1975).
  6. Eric R. Colby, "Design, Construction, and Testing of a Radiofrequency Electron Photoinjector for the Next Generation Linear Collider". Ph. D. Thesis, UCLA, 1997. See also SLAC-PUB-7946, 1998; J.P. Carneiro et al., "First Results of the Fermilab High-Brightness RF Photoinjector". Proceedings of the 1999 Particle Accelerator Conference, New York, NY (1999) p. 2027-2029.
  7. A.R. Fry, M.J. Fitch, A.C. Melissinos, B.D. Taylor, "Laser system for a high duty cycle photoinjector". Nuclear Instruments and Methods A430, 180 (1999).
  8. Craig W. Siders, Jennifer L.W. Siders, Antoinette J. Taylor, Sang-Gyu Park, and Andrew M. Weiner, "Efficient high-energy pulse-train generation using a  $2^n$ -pulse Michelson interferometer". Applied Optics 37, 5302 (1998).
  9. See for instance A. Yariv, "Optical Electronics". Holt Rinehart and Winston, New York 1985; chapter 9.

10. Ch.X. Tang, J. Ng, "Wakefields in the Beamline of TTF Injector II". TESLA Collaboration report 97-11, DESY (May 1997).



The crystal is mounted in the first cross downstream of the chicane.

Figure 1: The A0 photoinjector beam line. The location of the crystal with respect to r-f gun is indicated.



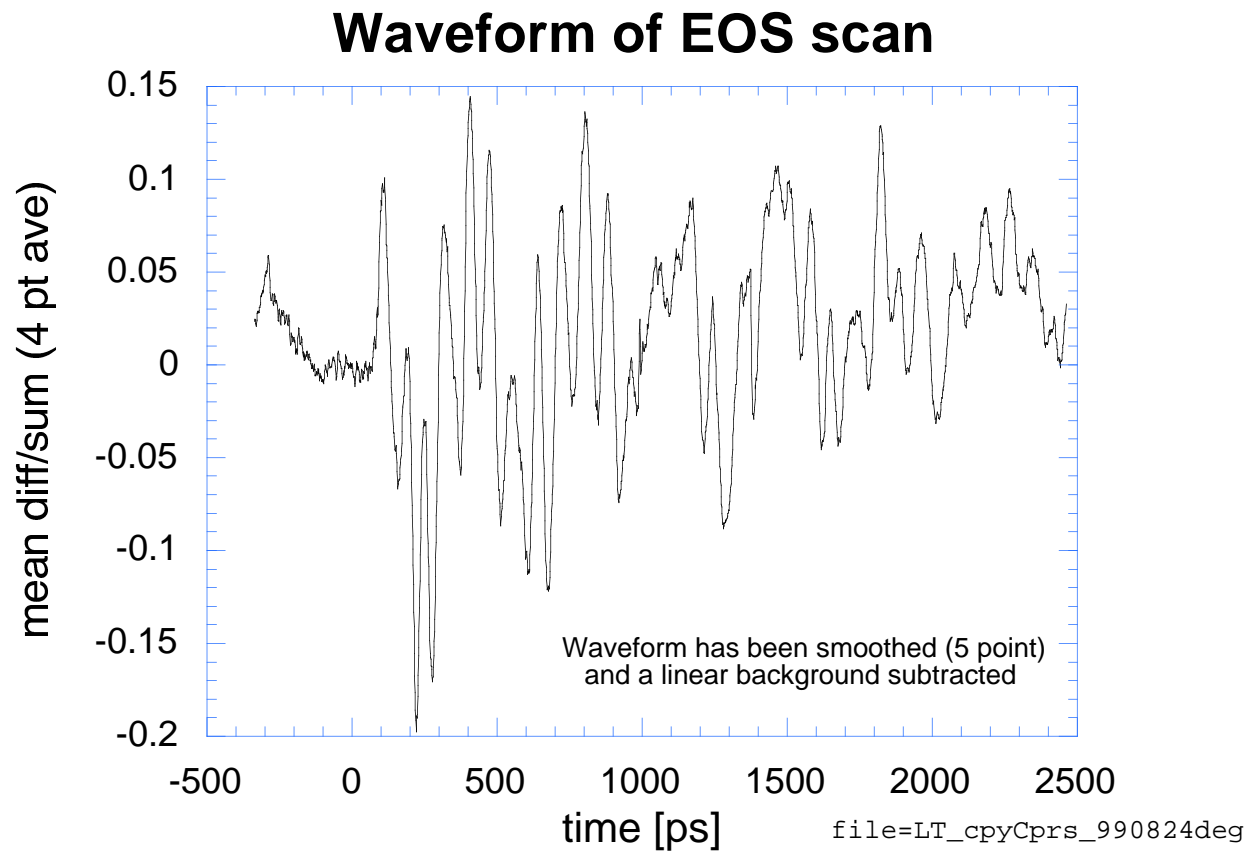


Figure 3: Measured tangential electric field at the eo crystal as a function of time after the arrival of the electron bunch. The ordinate represents the measured polarization asymmetry  $R = \sin \Gamma$  in 1 ps steps.

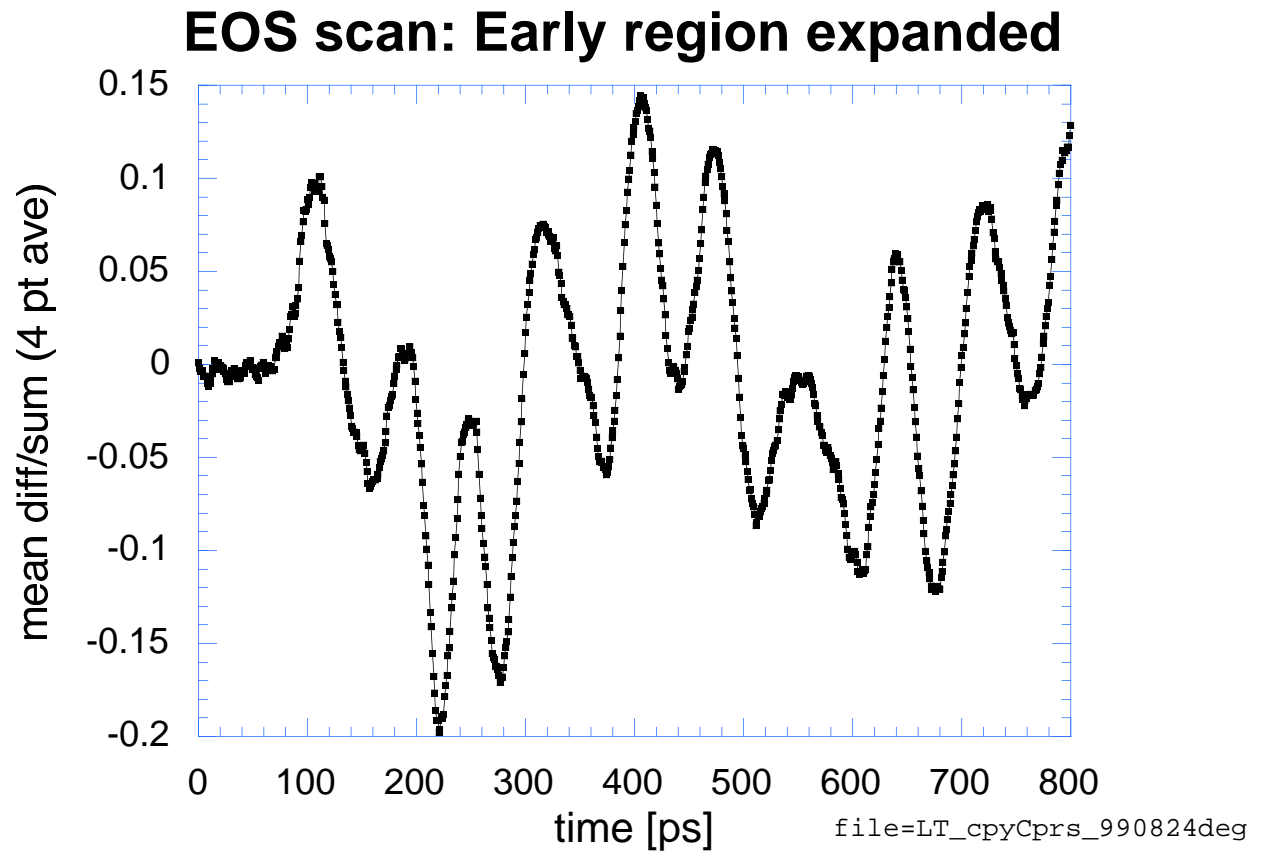


Figure 4: Same waveform as in Fig 3. but with the early region expanded.

### Gaussian fit to first peak in EOS scan

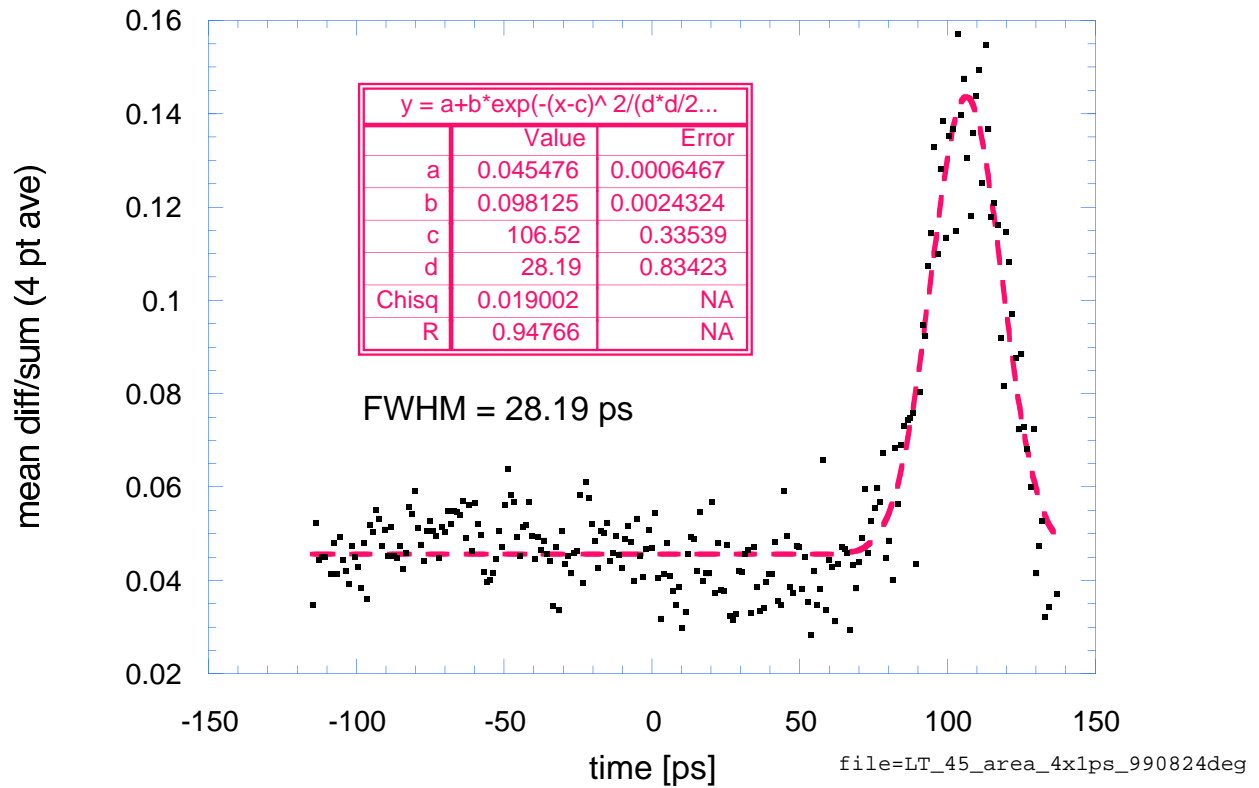


Figure 5: The first peak from the waveform in Fig 3. on an expanded scale with a Gaussian fit.

## Fast Fourier Transform of EOS scan

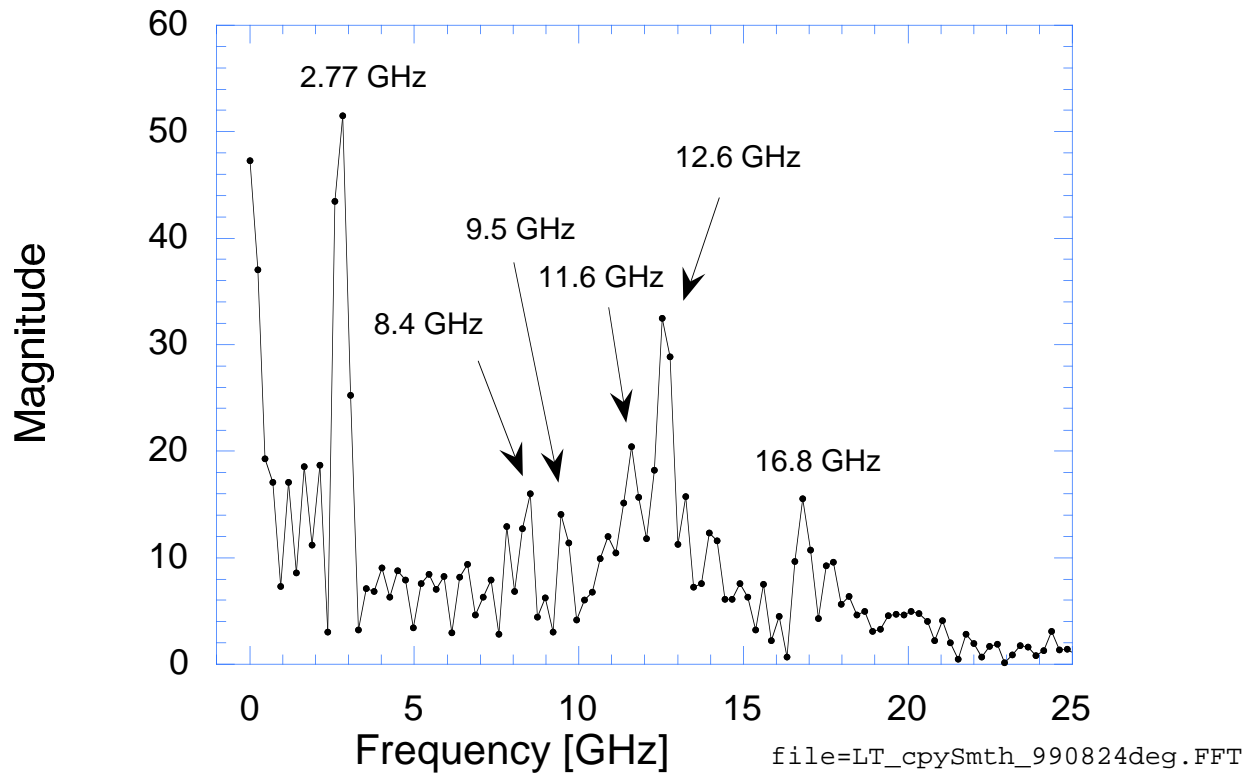


Figure 6: Fourier spectrum of the data shown in Fig. 3. Note the discrete frequencies as marked.